Digital Discovery

ROYAL SOCIETY OF CHEMISTRY

PAPER

View Article Online
View Journal | View Issue

Cite this: *Digital Discovery*, 2025, **4**, 3533

ReactPyR: a python workflow for ReactIR allows for quantification of the stability of sensitive compounds in air

Nicola L. Bell, * Emanuele Berardi, Marina Gladkikh, Richard Drummond Turnbull and Freya Turton

The digitalisation of air-sensitive chemistry remains an underexplored frontier, largely due to the binary and qualitative classification of compounds as either "air-sensitive" or "air-stable". This lack of quantitative data not only limits reproducibility and mechanistic understanding but also introduces significant time and cost burdens associated with unnecessary or overly cautious handling procedures. In this work, we present a modular digital workflow that integrates automated liquid handling, stirring, and *in situ* ReactIR spectroscopy to systematically assess and quantify the air-sensitivity of commercial hexamethyldisilazide salts. This approach enables reproducible, high-resolution degradation profiling and uncovers mechanistic trends that are unfeasible through conventional methods. Central to our workflow is *ReactPyR*, a Python package that provides programmable control of the ReactIR platform and seamless integration with digital laboratory infrastructure. Together, these advances demonstrate how automation can accelerate data collection to enhance the study and handling of reactive chemical systems.

Received 11th July 2025
Accepted 19th September 2025

DOI: 10.1039/d5dd00305a

rsc.li/digitaldiscovery

Introduction

Inline analytical tools are central to the digitalisation of chemical syntheses, enabling real-time monitoring, reproducibility, and feedback-driven optimisation of reactions.[1–5] For probing highly reactive species, non-destructive spectroscopies such as NMR, UV/vis, and IR are typically preferred over chromatographic or mass spectrometric techniques, due to their minimal sample perturbation and fine temporal resolution.[6] Among these, ReactIR (and its analogue, ReactRAMAN) is particularly versatile: applicable across diverse chemical systems *via* universal molecular vibrational signatures, and deployable in both probe-based and flow-cell configurations.[7] Its compatibility with a range of concentrations, temperatures, and reaction timescales makes it an attractive component for digitally integrated workflows. However, its wider adoption in modular digital chemistry platforms may be limited by the constraints of its proprietary control software.[8,9] To address this, we introduce *ReactPyR*, a Python package that enables external control of Mettler Toledo's iCIR software, facilitating seamless integration of ReactIR into automated workflows. We demonstrate this capability through the development of a robust methodology for quantifying the air sensitivity of organometallic reagents—an application that highlights the power of open, interoperable tools for broadening the applicability of digital chemistry.

Organometallic and metalorganic species are characterized by their high reactivity towards a range of substrates including the atmosphere under which their chemistry is conducted. This necessitates the use of specialised equipment (*e.g.*, gloveboxes and Schlenk lines) as well as techniques that are time-consuming, costly, and limited by the skills of the experimentalist.[10,11] These operational challenges can limit broader access to organometallic chemistry, particularly in high-throughput or industrial contexts where air-sensitivity can restrict the practical use of otherwise valuable compounds. As such, a significant body of research has focused on designing air-stable analogues—often through strategic modification of ligands or substituents, to preserve reactivity while enhancing robustness.[12–14] The digital lab revolution presents an opportunity to develop new tools which lower the barriers to entry for handling such compounds.[15–18]

In the chemical literature, compounds are commonly described in binary terms as either air-sensitive or air-stable (Fig. 1(top)). This simplistic classification belies the fact that rates of decomposition under reactive atmospheres are not static or absolute for either category, but reflective of underlying thermodynamic and kinetic factors (Fig. 1(bottom)). While quantitative metrics, such as degradation half-life, could in principle be used to characterise this behaviour, they are rarely measured, inconsistently reported, and have not been adopted as standard practice. As a result, data supporting a measurable

School of Chemistry, University of Glasgow, Glasgow, G12 8QQ, UK. E-mail: Nicola.Bell@Glasgow.ac.uk

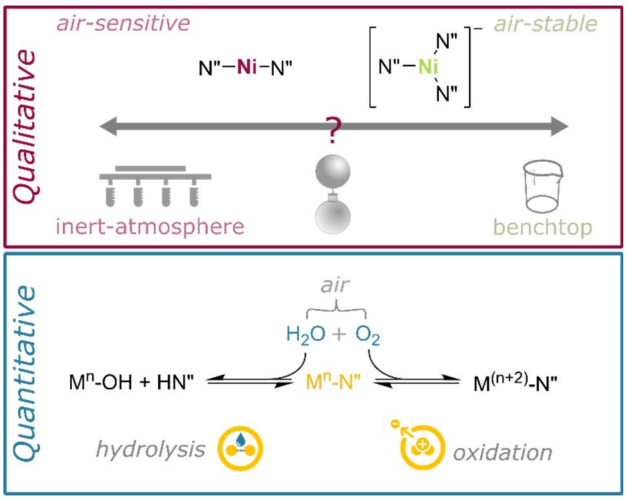

Fig. 1 (Top) Organometallics are often classified by a binary (air-sensitive/air-stable) fashion which belies the fact that some are more sensitive than others. However, the air-sensitivity of a species can dictate the technology, including digital tools, which must be used in its handling. (Bottom) Air-sensitivity derives from the reactivity of compounds towards the components of air, primarily oxygen and water vapour which should be quantifiable when used with a reproducible analysis methodology.

description of 'air sensitivity' remain sparse and determinations are, at best, anecdotal. Establishing and routinely applying such metrics would offer a more nuanced understanding of reactive species, guide safer and more efficient handling practices, and provide a framework for evaluating stabilisation strategies in a reproducible, data-driven manner.

A major challenge in developing a quantitative metric for air sensitivity lies in ensuring reproducibility across the many variables that influence degradation in air. These may include rate of air ingress, ambient temperature and humidity, solution surface area, stir rate, and stochasticity introduced by analytical sampling perturbations. Automation offers a powerful solution, enabling controlled, repeatable workflows for probing these complex processes. With this in mind, we set out to design a simple yet highly reproducible methodology for comparing relative degradation rates across a family of commonly used air-sensitive compounds. Air sensitivity consists primarily of two key reactions with the substrate: hydrolysis and oxidation. To demonstrate the process on hydrolysis first, we selected as a model compound the alkali metal hexamethyldisilazides (MHMDS, MN″, M = Li, Na, K), which undergo rapid hydrolysis in the presence of moisture but are largely unreactive toward aerobic oxidation. By integrating a liquid handling pump, a stirrer-hotplate, and automated periodic analysis using a ReactIR™ spectrometer, we developed a digital workflow for monitoring the degradation of HMDS salts under ambient conditions. Crucially, we also introduce ReactPyR, a Python package that provides programmatic control of ReactIR™, enabling seamless integration of this platform into modular, automated laboratory systems. The resulting data not only facilitate direct comparisons of relative air sensitivity but also offer new mechanistic insights into substrate instability under varied environmental conditions.

Methodology

Hardware

All experiments were conducted using a compact sampling setup designed for automated operation and regular looped spectroscopic monitoring. The system comprised a single LSP-One syringe pump (Advanced Microfluidics), a Mettler Toledo ReactIR™15 spectrometer equipped with a 50 μL flow cell, and custom designed, 3D-printed vial holder. Three separate vial positions allow for blank, sample and control vials for each run, which are positioned on an IKA RCT magnetic stirrer hotplate to ensure homogeneity during aspiration (Fig. 2).

The LSPOne pump utilises a 1 mL syringe and 12-port valve which allows for transfer of reagents from the vials and injection into the ReactIR Flow Cell as well as connecting cleaning stock solutions and waste output for system shutdown. All fluidic connections were made using chemically resistant PTFE tubing (1/16″ OD), ensuring chemical compatibility with organic solvents and substrates. Following the measurement of an initial spectrum, air was inlet to the system through an 18G syringe needle throughout the remainder of the experiment.

Software

To enable programmatic access and autonomous control of our inline ReactIR™ system we developed ReactPyR, which communicates with the spectrometer through an Open Platform Communications Unified Architecture interface (OPC UA).

OPC UA is a cross-platform, service-oriented communication standard designed for secure and reliable exchange of data. In the case of the ReactIR system, Mettler provide an OPC UA client server, exposing a structured address space that includes instrument state, spectroscopic outputs, and control parameters. Through this architecture, external clients can interact with the ReactIR device without requiring low-level hardware access.

ReactPyR is implemented using the asyncua Python library[19] and functions as a dedicated OPC UA client. Upon initialisation, it connects to the iCIR software's OPC UA endpoint, authenticates the session, and dynamically explores the server's address

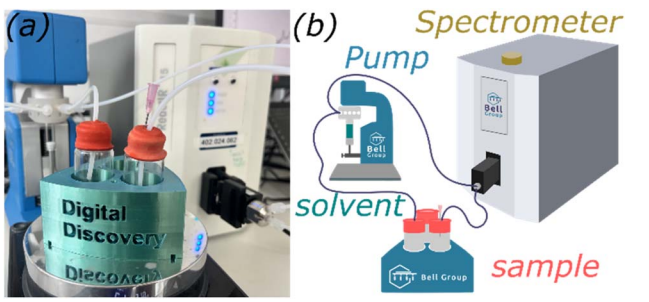

Fig. 2 Hardware setup for the experiment. (a) Photo of the setup during an experimental run. (b) Depiction of liquid connectivity in the setup.

space to identify relevant nodes corresponding to acquisition parameters (*e.g.*, scan interval, resolution), and system status (*e.g.* last background date). Using this interface ReactPyR is able to connect to the hardware, start experiments, set the interval of spectral collection, pause and resume experiments, collect spectral data, output data in labelled .csv format and safely shutdown the system.

Standard experimental setup protocol

A solution of the silylamide reagent in the solvent (3 mL) was prepared to the appropriate concentration. If necessary, an additive (*e.g.* TMEDA) was added with stirring. A second vial containing *ca.* 5 mL of neat solvent was also prepared. Both vials were capped with virgin Suba Seals and removed from the glovebox. The solvent vial was connected first to the LSPOne pump and the sample vial was connected directly to the flow cell head of the ReactIR *via* the outlet port (Fig. 2b). The 'Sensing sensitivity' experiment script was triggered. After the first sample spectrum was obtained, air was inlet to the system by insertion of an 18 G bleed needle.

Workflow development

To successfully integrate ReactPyR into our experimental workflow, it was essential to coordinate liquid handling and stirring with spectral data acquisition from the ReactIR system. Whilst regular aspiration and dispensing of the sample was desirable to facilitate air exposure, actively flowing solutions were observed to produce different signal intensities compared to static samples, likely due to differences in mixing, optical path stability, or flow dynamics. In addition, the ReactIR system operates on a fixed internal timing cycle, however key parameters such as the total acquisition time or precise end time are not accessible *via* the iCIR software, making it challenging to coordinate with other automated processes. To address both challenges, we designed a system where spectral acquisition is explicitly triggered by the completion of each liquid transfer step, rather than relying on passive, time-based acquisition.

Each experiment begins with the automated delivery of solvent to the ReactIR™ flow cell, followed by triggering the experiment to begin *via* ReactPyR (Fig. 3). A background

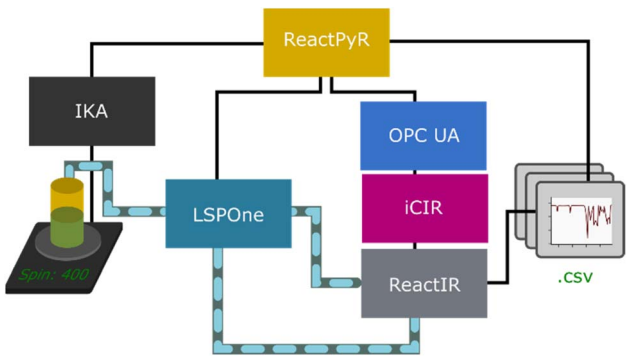

Fig. 3 Software and hardware connections show how the system is controlled.

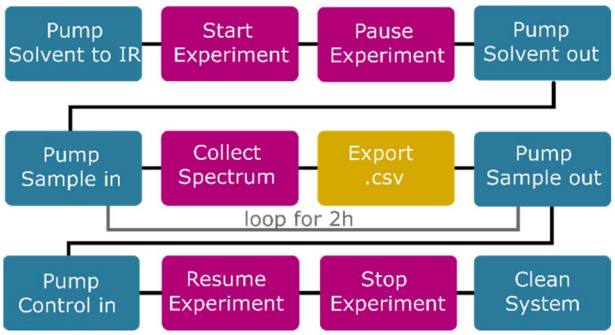

Fig. 4 Workflow for sensing sensitivity experiment. Clean system includes pumping of solvent, water, solvent and air sequentially to clear pump and ReactIR flow cell of substrate. Pump functions: blue; ReactPyR functions: pink; data functions: yellow.

spectrum is thus collected, after which acquisition is paused to transfer the analyte solution to the cell for sample acquisition. Following the initial scan, the sample is dispensed back into its stirred vial and a needle is inserted to introduce air into the system. This cycle—aspiration, spectral acquisition, and dispensing—repeats at each time point (Fig. 4), introducing air in a controlled, reproducible manner to drive hydrolysis. After two hours, an optional control solution may be added (*vide infra*), before the experiment concludes with automated cleaning of both the pump and flow cell. Throughout the experiment, spectra are continuously exported as comma-separated values (.csv) files for downstream processing and analysis.

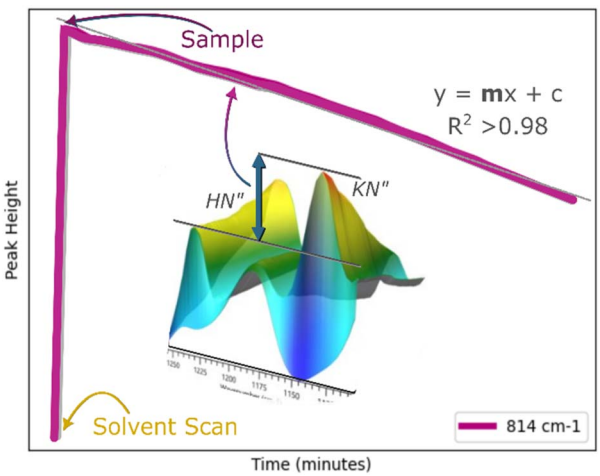

Fig. 5 Example run showing the peak height *vs.* time for substrate peak at 814 cm^{-1}. For all data peak height is determined by comparison of amide : amine band height at each time point (see inset 3D spectral plot). The first scan (solvent can) collects the intensity at this energy for the solvent blank. The second scan (sample) begins with 100% amide before air is inlet to the system and the pseudo zeroth-order degradation can be fit with a straight line, the gradient of which (*m*) yields the degradation rate. The inset 3D plot shows a region of the spectra (absorbance *vs.* energy) obtained from a run with the third axis representing time, thus we observe the KN″ (1132 cm^{-1}) signal intensity depleting while HN″ (1230 cm^{-1}) grows along the time axis.

Data analysis

Data analysis may be conducted either in the iCIR software or through processing of raw .csv data which is output in real-time during the course of each run. For convenience we have provided scripts for processing this raw data on the 'Sensing Sensitivity' GitHub repository (link below). The collection of a solvent sample at the beginning of the experiment allows for facile detection of relevant substrate bands by spectral subtraction (Fig. 5). Changes in relative amide : amine (MN″ : HN″) absorption were plotted at 2 minute intervals for up to four different signature bands in each sample, with the highest-intensity band typically arising at *ca.* 814 cm^{-1}, corresponding to the Si–Me rocking vibration.[20] Because the degradation was always observed to be pseudo-zeroth order, least-squares analysis of the trendline for normalised substrate peak height over time yielded the relative rate of degradation for each. To validate the accuracy of substrate peak measurements (and thence calculated half-lives) across different solvents, control samples consisting of 50/50 mol% [HMDS] : [KN″] were added at the end of each solvent variation experiment (see SI for further details).

Results and discussion

Exposure of potassium hexamethyldisilazide (KN″, KHMDS) in THF solvent (333 μM) to air over the course of 2 h revealed key absorption bands at 814 cm^{-1} (RSD 2%, Si–Me rock[20]) and 1134 cm^{-1} (RSD 3%), alongside a weaker band at 1232 cm^{-1} (RSD 6%, CH_3 symmetric deformation) observed with slightly poorer precision (over 4 repeat runs). Our data appeared to show a moderate negative correlation, which was not statistically significant, between ambient humidity and degradation rate (Table S2 and Fig. S2). Similarly, for temperature a non-significant correlation was observed (Fig. S3). These data suggest that moderate in-lab variations have much more subtle effects than the parameters studied below. Therefore, for all of our experiments humidity and temperature was recorded but not controlled. The 'initial' rate of decay of KN″, which the sample exhibited for the duration of our experiments (2–4 h), was found to follow pseudo-zeroth order kinetics.[21] This could be rationalised as arising from the minimal local concentration of water vapour in solution, which is continuously replenished from the atmosphere whilst a significant excess of the substrate is maintained. The reaction of LiN″ with water has previously been shown to be close to barrierless, in gas phase studies where the amide is monomeric, even at ultracold conditions.

Varying the initial concentration of the substrate in our samples allowed us to determine a true reaction order of −1 with respect to KN″ (Fig. 6b). Thus increasing the initial concentration of our substrate decreased the rate of degradation. This data is likely indicative of a pre-equilibrium step in which the active species, KN″, interconverts with a less reactive form; which may suggest that the cleavage of a dimer is responsible, with only (or principally) monomeric KN″ participating in the degradation reaction (see SI for potential mechanism). It is well-established that alkali metal silylamide reagents exist in various solvation states and aggregates in solution, and that dimeric forms are particularly thermodynamically favoured in non-chelating media (Fig. 7).[22–26]

Comparison of equimolar solutions of LiN″, NaN″, and KN″ in THF (333 μM) found the former to be the least reactive towards adventitious water, with a half-life 3.4 times that of KN″ while for the sodium cation the half-life was calculated to be 2.5 times that of the larger ion (Fig. 6a). These observations are consistent with the trend in polarizabilities[27] of the associated alkali metal cations (Fig. 6a, inset), as well as a looser correlation with electronegativity[28,29] and ionic radius (Table S3). All three of these factors presumably influence their aggregation behaviour.

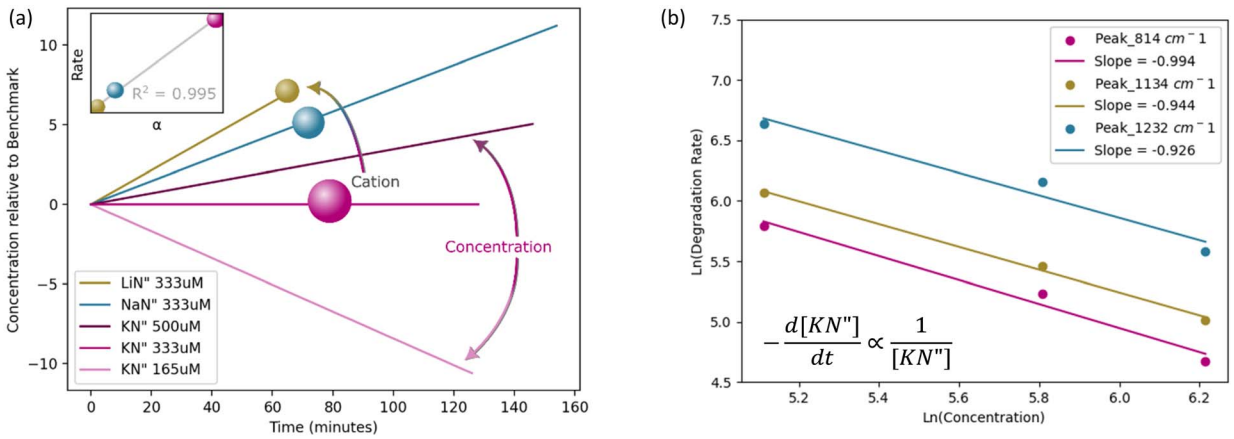

Fig. 6 (a) Effect of cation and concentration on degradation of amide relative to the benchmark sample (KN, 333 μM in THF, see Fig. 5). Coloured spheres represent different cations with their size representing ionic radius (yellow sphere: lithium; blue sphere: sodium; purple sphere: potassium) inset: plot of electronegativity (χ) *versus* degradation rate for MN″ compounds demonstrating a linear relationship. Spheres coloured as in main chart. (b) Plot of Ln(concentration) *vs.* Ln(degradation Rate) for three different bands in the IR spectrum demonstrating the negative first order dependence of degradation rate on concentration of the silylamide for three different concentrations. Inset equation for the dependence of degradation rate on KN″ concentration.

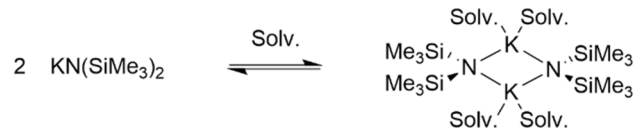

Fig. 7 Equilibrium of dimer and monomer of potassium hexamethyldisilazide.

Some of the aforementioned absorption bands were not clearly identifiable in other solvents, therefore, in order to ensure our comparisons remained valid when studying different solvent systems, a control spectrum containing HMDS (0.5 equiv.) and KN″ (0.5 equiv.) was collected at the end of each solvent scope experiment. From the substrate band intensity value ($y_{1/2}$) and the linear pseudo-zeroth order fit of the degradation ($y = mt + c$) we could find the first half-life ($t_{1/2}$) at observed $y_{1/2}$ for each solvent. From this work, the empirical half-life can be compared to the one calculated from the rate constant (k) of the pseudo-zeroth order initial phase. In this fashion the half-life in THF was measured to be 3.9 h (calcd 3.6 h from k, Table 1) which was close to the value obtained for DME. In contrast, the half-life in toluene was found to be 6.6 h, which may reflect an equilibrium which strongly favours dimerisation of the substrate. Surprisingly, KN″ in fluorobenzene behaves very differently with a half-life of only 2.4 h which may indicate solvent degradation.[30] Whilst diethyl ether and 2-methyl THF proved challenging to study due to evaporation and aerobic oxidation respectively, cyclopentylmethylether (CPME) was found to accelerate degradation relative to the other ethereal examples. Chelating additives dramatically affected degradation rates in THF, lending considerable further credence to the argument for a strong dependence of degradation rates on solution-phase aggregation effects. Addition of 18-crown-6 produced an eightfold increase, whilst more flexible PMDETA

Table 1 Relative first half-lives derived from our experiments determined under the conditions below

		Half-life (h)	
Reagent	Variable	Exp.[c]	Calc.[d]
KN″	166 μM	3.9	3.6
	333 μM	—	13.4
	500 μM	—	28.2
NaN″	Na	—	33.3
LiN″	Li	—	46.2
KN″	Toluene[a]	6.6	6.9
	FPh[a]	2.4	2.6
	CPME	2.3	2.8
	DME[a]	5.0	5.0
	DME[b]	5.4	6.2
	TMEDA[b]	7.7	7.9
	PMDETA[b]	1.4	0.8
	18-Crown-6[b]	1.3	0.9

[a] Neat. [b] 1 equiv. [c] $y_{1/2}$ measured for sample containing 0.5 amide : 0.5 amine and $t_{1/2}$ calculated from the pseudo-zeroth order fit line ($y = mt + c$) of the degradation data. [d] $t_{1/2} = [N''_0]/2k$.

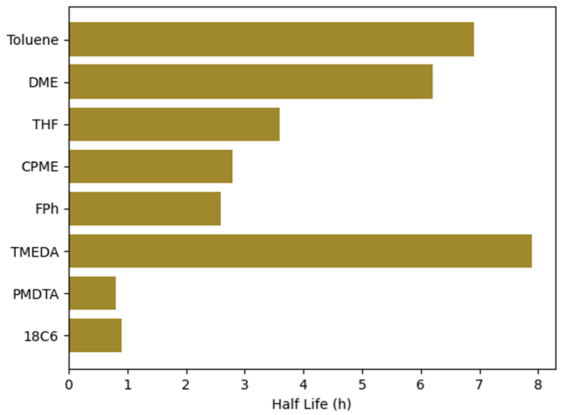

Fig. 8 Experimentally determined half-lives (hours) of KN″ (166 μM) in different solvents and chelators studied (see SI for half-life calculation).

quickened the rate of degradation by an order of magnitude. In contrast, even stoichiometric quantities of DME in toluene have a much less pronounced effect, and—most strikingly—addition of TMEDA in fact reduced the degradation rate relative to neat toluene. It is strongly implied that the remarkable stability of the $\{(TMEDA)KN''\}_2$ dimer is responsible for the divergent behaviour of this system (Fig. 8).[22]

Based on the above data we hypothesised that the presence of excess cations in solution may promote aggregation and aid stabilisation of the silylamide complexes. Therefore, addition of sub-stoichiometric amounts of alkali metal salts (MX = LiCl, KCl and $LiNTf_2$) was investigated. Solutions of KN″ with either 5 or 20 mol% added salt were stirred for 3 days in THF prior to analysis to ensure maximal dissolution of the salts. Notably no HMDS was observed after this time indicating degradation had not taken place during inert atmosphere stirring. Upon subsequent exposure to air of these samples it was immediately clear that precipitation of some of the silylamide had occurred with the peak intensity for the amide peak being reduced by up to 30% relative to the benchmark. Analysis showed a small

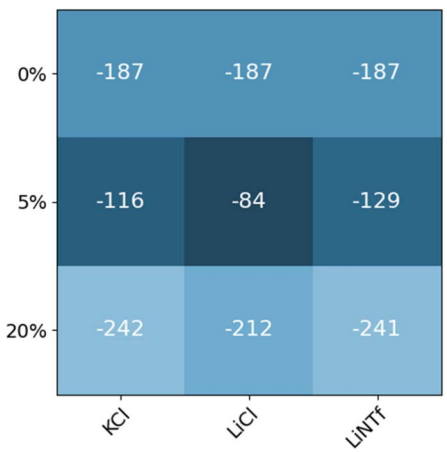

Fig. 9 Heat map of the variation in reaction rate with salt additives shows a non-linear relationship with small quantities decreasing degradation while larger quantities promote it.

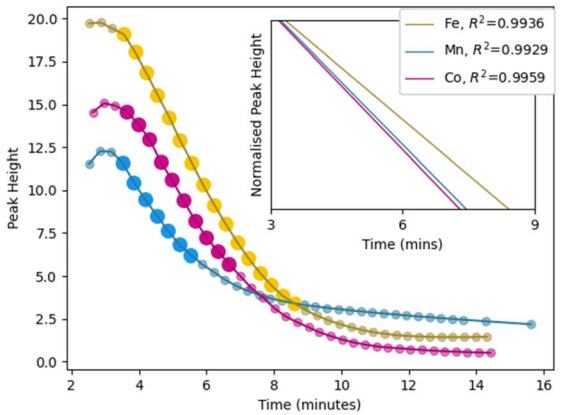

Fig. 10 Plot of the degradation of the band between 970–990 cm^{-1} in spectra of FeN''_2 (yellow), MnN''_2 (blue) and CoN''_2 (purple) in toluene (166 μM). The linear region is highlighted with enlarged scatter points in each. Inset: best fit lines for normalised peak height *vs.* time during the pseudo-first-order period only (large points in main chart) for the same experiments showing the R^2 value for the linear fit of each data set.

positive effect of 5 mol% MX salts but a negative effect for the 20 mol% examples (Fig. 9). Silylamides are known to form inverse crown structures with halide salt however this has not been observed with triflimides.[31] Precipitation of a portion of the substrate results in lower solution concentrations of the solvated silylamides in solution which will then be expected to degrade faster due to the shift in equilibrium at lower concentration, as noted above. Despite this the data does reveal that small additive quantities can have a mitigating effect on degradation rate.

In a further demonstration of the potential of this methodology, we investigated the degradation of a set of redox-active transition metal silylamides, MnN''_2, FeN''_2, CoN''_2. These complexes are paramagnetic, complicating their analysis by other spectroscopic techniques and demonstrating the power of IR in these examples. The degradation of these samples was found to be significantly more rapid than the alkali metal hydrolysis analogues and thus spectra were collected at 15-second intervals, rather than the 2-minute intervals for the above. A key band at 970–990 cm^{-1} was present in all three substrates (Fig. S25). Analysis of this band over time reveals rapid degradation within <6 min (Fig. 10). From this data we can extract a pseudo-zeroth order period where intensity correlates linearly with time for all three samples. Normalising these data for intensity allows us to compare the rate of degradation for the three samples (Fig. 10 inset). Degradation was slowest for the iron complex (Fig. 10 inset, yellow) while the rate was very similar for Mn (Fig. 10 inset, blue) and Co (Fig. 10 inset, purple), although slightly slower for the latter. These values track the relative oxidation potentials of the divalent ions (Co: +1.8 V; Mn: +1.5 V; Fe: +0.77 V) indicating that this degradation may reflect an aerobic oxidation mechanism rather than hydrolysis.

Conclusions

Measured rates of the aerobic degradation of hexamethyldisilazide salts are straightforwardly, and quantitatively, obtained by continuous observation *via* solution-phase infrared spectroscopy, revealing several trends linked to the dynamic structural changes experienced by substrates in solution. Whereas studies indicate a negative reaction order (in substrate initial concentration), hydrolysis generally proceeds, in the initial period, according to pseudo-zero-order rate laws for extended durations. Relative reaction rates correlate inversely with polarizability of the substrate cation, with the lithium analogue degrading significantly less quickly than its heavier congeners; however, the introduction of sub-stoichiometric quantities of other alkali metal salts produces a non-linear effect, with small amounts improving stability but degradation accelerating at higher concentrations. Substrate half-lives are also extended in toluene compared to ethereal solvents, whereas strong chelators such as PMDETA and 18-crown-6 accelerate degradation considerably. Perhaps most significant, though, is the effect of introducing TMEDA, which has a dramatically stabilising effect on KN″ in toluene—probably due to the formation of remarkably stable, dimeric $[KN''(TMEDA)]_2$.

Collection of these data was made possible by ReactPyR, our Python package enabling digital control of Mettler Toledo's ReactIR spectrometers. By integrating ReactIR with liquid handling and stirrer-hotplate modules under automated control, this approach minimises variability in the control of experimental conditions to achieve a level of consistency and data quality which is difficult to achieve by manual methods.

ReactPyR enables ReactIR™ to be integrated flexibly into modular digital workflows, allowing spectroscopic data to be collected and synchronized with upstream and downstream operations. This modularity is especially powerful for air-sensitive chemistry, where conventional digital workflows are often inadequate. The reproducible handling of highly reactive systems requires bespoke digital strategies that account for their sensitivity to environmental variables. Our work illustrates how modular, programmable approaches—such as those enabled by ReactPyR—can expand the reach of digital chemistry into more complex experimental spaces, where bespoke workflows are essential for safe, efficient, and reproducible discovery.

Author contributions

N. B. obtained the funding, devised the project, conducted method development, collected the concentration and cation data and wrote the manuscript. E. B. wrote the ReactPyR and Sensing Sensitivity code. M. G. wrote the data analysis code and the modified the liquid handling base code from Advanced Microfluidics. M. G. also conducted the solvent screen and synthesised the transition metal silylamides. R. D. T. conducted the salt addition studies and helped write the manuscript. F. T. conducted the studies involving stoichiometric chelator addition.

Conflicts of interest

There are no conflicts to declare.

Data availability

All code associated with ReactPyR (latest release) can be found at **https://github.com/Bell-Group-Glasgow/ReactPyR**. The archived version at the time of publication (v1.0.0) is available *via* Zenodo: **https://doi.org/10.5281/zenodo.17159492**. Similarly, code associated with the experiments detailed herein (latest release) can be found at **https://github.com/Bell-Group-Glasgow/SensingSensitivity**. The archived version at the time of publication (v1.0.0) is available *via* Zenodo: **https://doi.org/10.5281/zenodo.17159501**. All code is provided subject to a Creative Commons CC-BY-NC license.

Supplementary information: further experimental data, including charts and data tables. See DOI: **https://doi.org/10.1039/d5dd00305a**.

Acknowledgements

This work was supported by the Engineering and Physical Sciences Research Council through the award of an EPSRC Open Fellowship to NB (EP/W02702X/1) and by the University of Glasgow *via* Lord Kelvin Adam Smith Fellowship funds. This work was also supported by a Royal Society Research grant (RG\R2\232338). MG and FT acknowledge the EPSRC for DTA funding (EP/W524359/1).

References

1 A. J. S. Hammer, A. I. Leonov, N. L. Bell and L. Cronin, *JACS Au*, 2021, **1**, 1572–1587.
2 M. Christensen, L. P. E. Yunker, P. Shiri, T. Zepel, P. L. Prieto, S. Grunert, F. Bork and J. E. Hein, *Chem. Sci.*, 2021, **12**, 15473–15490.
3 B. P. MacLeod, F. G. L. Parlane, A. K. Brown, J. E. Hein and C. P. Berlinguette, *Nat. Mater.*, 2022, **21**, 722–726.
4 T. Hardwick and N. Ahmed, *Chem. Sci.*, 2020, **11**, 11973–11988.
5 J. Tschudi, M. O'Farrell and K. A. Hestnes Bakke, *Appl. Spectrosc.*, 2018, **72**, 1298–1309.
6 J. B. M. Parambath and A. A. Mohamed, *Characterization Techniques of Organometallic Compounds in Organometallic Compounds*, 2023, pp. 245–266, DOI: **10.1002/9783527840946.ch12**.
7 C. F. Carter, H. Lange, S. V. Ley, I. R. Baxendale, B. Wittkamp, J. G. Goode and N. L. Gaunt, *Org. Process Res. Dev.*, 2010, **14**, 393–404.
8 P. Sagmeister, R. Lebl, I. Castillo, J. Rehrl, J. Kruisz, M. Sipek, M. Horn, S. Sacher, D. Cantillo, J. D. Williams and C. O. Kappe, *Angew. Chem., Int. Ed.*, 2021, **60**, 8139–8148.
9 R. Chung and J. E. Hein, *React. Chem. Eng.*, 2019, **4**, 1674–1681.
10 A. M. Borys, *Organometallics*, 2023, **42**, 182–196.
11 R. J. Errington, *Advanced Practical Inorganic and Metalorganic Chemistry*, CRC Press, London, 1997.
12 L. Nattmann, R. Saeb, N. Nöthling and J. Cornella, *Nat. Catal.*, 2020, **3**, 6–13.
13 G. McArthur, J. H. Docherty, M. D. Hareram, M. Simonetti, I. J. Vitorica-Yrezabal, J. J. Douglas and I. Larrosa, *Nat. Chem.*, 2024, **16**, 1141–1150.
14 A. M. Borys and E. Hevia, *Organometallics*, 2021, **40**, 442–447.
15 N. L. Bell, F. Boser, A. Bubliauskas, D. R. Willcox, V. S. Luna and L. Cronin, *Nat. Chem. Eng.*, 2024, **1**, 180–189.
16 N. L. Bell, M. Gladkikh, C. Fraser, M. Elsayed, E. Richards and R. D. Turnbull, *Angew. Chem., Int. Ed.*, 2025, e202505408.
17 S. C. Smith, C. S. Horbaczewskyj, T. F. N. Tanner, J. J. Walder and I. J. S. Fairlamb, *Digital Discovery*, 2024, **3**, 1467–1495.
18 A. N. Lebedev, K. S. Rodygin, S. A. Vakhrusheva and V. P. Ananikov, *Green Chem.*, 2024, **26**, 3776–3785.
19 **https://github.com/FreeOpcUa/opcua-asyncio**.
20 K. Nakamura, H. Nonaka, N. Kameda, T. Nishiguchi and S. Ichimura, *Jpn. J. Appl. Phys.*, 2008, **47**, 7349.
21 L. Pogliani, *React. Kinet. Catal. Lett.*, 2008, **93**, 187–191.
22 J. A. Spivey and D. B. Collum, *J. Am. Chem. Soc.*, 2024, **146**, 17827–17837.
23 R. A. Woltornist and D. B. Collum, *J. Org. Chem.*, 2021, **86**, 2406–2422.
24 A. I. Ojeda-Amador, A. J. Martínez-Martínez, G. M. Robertson, S. D. Robertson, A. R. Kennedy and C. T. O'Hara, *Dalton Trans.*, 2017, **46**, 6392–6403.
25 O. Tai, R. Hopson and P. G. Williard, *J. Org. Chem.*, 2017, **82**, 6223–6231.
26 M. P. Coles, *Coord. Chem. Rev.*, 2015, **297–298**, 2–23.
27 B. R. Eichelberger, T. P. Snow and V. M. Bierbaum, *J. Am. Soc. Mass Spectrom.*, 2003, **14**, 501–505.
28 H. Y. Leng, T. Ichikawa, S. Hino, N. Hanada, S. Isobe and H. Fujii, *J. Power Sources*, 2006, **156**, 166–170.
29 D. W. Barnum, *Inorg. Chem.*, 1983, **22**, 2297–2305.
30 T. L. Gilchrist, *Product Class 3: Arynes, in Category 6, Compounds with All-Carbon Functions*, Georg Thieme Verlag KG, Stuttgart, 1st edn, 2008, vol. 43.
31 A. R. Kennedy, R. E. Mulvey, C. T. O'Hara, G. M. Robertson and S. D. Robertson, *Angew. Chem., Int. Ed.*, 2011, **50**, 8375–8378.